SPECTRAL CHARACTERISTICS OF FLASH FLOOD AREAS FROM MEDIUM SPATIAL OPTICAL IMAGERY

Muhammad Priyatna[1]*, Muhammad Rokhis Khomarudin[1], Galdita Aruba Chulafak[1], Sastra Kusuma Wijaya[2]

[1]Remote Sensing Applications Center, Indonesian National Institute of Aeronautics and Space (LAPAN)
[2]Universitas Indonesia
*e-mail: muhammad.priyatna@brin.go.id/mpriyatna@yahoo.com

Abstract. This study aims to investigate surface reflectance changes over flash flood areas in Nusa Tenggara Timur, Indonesia. Fifteen sample points from Sentinel-2 satellite imagery were used to analyse the differences in reflectance of areas before and after flash flood events. The method used involved analysis of the significant differences in the dreflectance values of each Sentinel-2 channel. The analysis results show that channels 6, 7, and 8A displayed significant differences compared to the others with regard to reflectance before and after flooding, for both settlements and shrubs. The results could be used for further research in building a reflectance index for the rapid detection of affected areas, with a focus on these channels.

Keywords: *reflectance, flash flood, disaster, bush, settlement*

1   INTRODUCTION

Flash floods are events that occur briefly (Adi Seno, 2013). They can occur due to heavy rainfall or as the result of the collapse of natural embankments or man-made structures (Larsen et al., 2001). Some examples of flash floods include events in Bogor and Lebak regencies in 2020, in Manado in 2014, and in NTT in 2021.

On April 4, 2021, tropical storm Seroja caused a major disaster in Indonesia and Timor Leste, particularly in the Province of East Nusa Tenggara (NTT), Indonesia (Aryaseta, 2021; Cleenewerck, 2021). The precursor of cyclone Seroja formed in the Sawu Sea on April 3, 2021, moving and strengthening southward towards Australia. The cyclone brought heavy rain to the NTT region and caused floods, landslides, and flash floods (Aryaseta, 2021). Flash floods occurred in

East Flores Regency (Ile Boleng, East Adonara, and Wotan Ulumado), Lembata Regency (Ile Ape and East Ile Ape), and Alor Regency (Aryaseta, 2021). The area most affected was Nelelamadike Village, Ile Boleng District, East Flores Regency, with the death toll of around 50 people. Most flash floods occur on the slopes/foot of volcanoes, such as Mount Ili Boleng and Mount Ili Lewotolok. Mount Ili Boleng is located in the southeastern part of Adonara Island (Helfinalis et al., 2012).

In order to provide information on areas affected by flash floods, it is necessary to map them. One of the most effective ways to map flash flood areas is by using remote sensing data, which can observe a reasonably large area as well as inaccessible locations (Waru et al., 2020). Two techniques are commonly used for obtaining space-based mapping information. The first is by using visual

163

interpretation based on before and after images of flash flood events, then manually digitising the changed or affected area. The second technique is to employ a digital approach using reflectance values in areas affected by flash floods, based on their physical characteristics identified from remote sensing satellite data. The visual interpretation technique can produce more accurate results than digital classification, but it is time consuming and need human expertise, which is subjective (Panigrahy et al., 2010).

Spectral reflectance values can be used to detect objects using remote sensing imagery, such as observing water bodies in floodplain areas during flood and low tide periods using Hyperion data (Rudorff et al., 2009); observing the most influential channels for detecting burnt areas, vegetation, and open land using LANDSAT, IKONOS, and ASTER images (Pleniou & Koutsias, 2013); and by estimating the burnt areas from AVHRR images (Razafimpanilo et al., 1995).

Detection of flood-affected areas has been made using a spectral transformation approach, such as the Normalized Difference Vegetation Index (NDVI) (Ahmed & Akter, 2017); the Normalized Difference Water Index (NDWI) (Khalifeh Soltanian et al., 2019); the Enhanced Vegetation Index (EVI) (Islam et al., 2010); and the Land Surface Water Index (LSWI) (Islam et al., 2010). The latter was employed to detect floods in Bangladesh using MODIS imagery (Islam et al., 2010), as well as the use of Normalized Difference Surface Water Index (NDSWI) with EO-1 ALI and Landsat TM images (Amarnath, 2014). Using low-resolution satellite imagery will have opportunity in temporal resolution, but it will be difficult to use if the affected area is not very wide.

One of the remote sensing satellites that can be used for monitoring is Sentinel-2. This is a European Space Agency (ESA) satellite that uses optical sensors (Drusch et al., 2012; Wang et al., 2016), with a temporal resolution of 10 days in the equatorial region. However, since 2017, Sentinel-2 has included two satellites, Sentinel-2A and Sentinel-2B, resulting in a temporal resolution of five days for the equatorial region using a constellation with a phase delay of 180° in the same orbit (Drusch et al., 2012). With this temporal resolution, monitoring of an area will be easier. Sentinel-2 can be used to quickly determine disaster-affected areas, especially when high-resolution data cannot be obtained. The use of Sentinel-2 instead of Landsat-8 caused by the selection of the data is easier and the acquisition time can be as near as the event time. Landsat-8 has a 16-day temporal resolution, which means that data can be acquired up to 16 days after an event has occurred, but this can be more of a problem if the area of interest is covered by cloud.

The purpose of this study is to investigate spectral reflectance changes before and after the occurrence of flash floods from medium spatial resolution imagery and to analyse the surface reflectance based on the physical behaviour of the electromagnetic spectrum over objects in the flash flood area.

2 MATERIALS AND METHODOLOGY
2.1 Study area

The study area was Nelelamadike Village, Ile Boleng District, East Flores Regency, East Nusa Tenggara Province, Indonesia, as shown in Figure 2-1. The study area was the worst affected by flash floods due to tropical storm Seroja in 2021. These occurred on April 4, 2021 in

Nelelamadike Village, with the acquisition of Sentinel-2 data related to the flash flood area on April 8, 2021. It was possible to acquire the cloud-free data quickly because the cause of the disaster was a tropical cyclone, which occurred in April. In the East Nusa Tenggara region, April is the beginning of the dry season, so after the occurrence of a tropical cyclone, weather conditions will return to normal with minimal cloud formation (Giarno et al., 2012; Trainor, 2002). If a flash flood event is caused by heavy rainfall occurring during the rainy season, in that case the observation site will often be covered by cloud, and it could take weeks or even months to obtain the first cloud-free optical sensing data after the event.

2.2   Data

The remote sensing data used were Sentinel-2 imagery. Sentinel-2 has 13 channels divided into visible, near-infrared, and short wave infrared ones (Zhang et al., 2017). Its images have several spatial resolutions, of 10 m, 20 m, and 60 m, with a coverage area of a width of 290 km (Drusch et al., 2012). The orbit of Sentinel-2 is Sun-synchronous at an altitude of 786 km (488 mi), and a recording time of 10:30 a.m. for the descending node (Claverie et al., 2018; Main-Knorn et al., 2017; Traganos & Reinartz, 2018). This local time was chosen as a compromise to minimise cloud cover and obtain appropriate solar lighting (Spoto et al., 2012). The time approximates to the local Landsat recording time and exactly matches the SPOT recording time, which allows for a combination of Sentinel-2 data and historical imagery to construct long-term time series (Claverie et al., 2018; Gascon et al., 2014; Martimort et al., 2007). Table 1 shows a comparison between Sentinel-2A and Sentinel-2B wavelengths (Doshi et al., 2020). The satellites have different wavelength centres, although the difference is not great. For comparison, the bandwidth between bands is also mostly the same, although there are some differences, namely band 5 (1 nm), band 8a (1 nm), band 9 (1 nm), band 10 (1 nm), band 11 (3 nm), band 11 (3 nm), and band 12 (10 nm).

The remote sensing data used were Sentinel-2 imagery. Sentinel-2 has 13 channels divided into visible, near-infrared, and short wave infrared ones (Zhang et al., 2017). Its images have several spatial resolutions, of 10 m, 20 m, and 60 m, with a coverage area of a width of 290 km (Drusch et al., 2012). The orbit of Sentinel-2 is Sun-synchronous at an altitude of 786 km (488 mi), and a recording time of 10:30 a.m. for the descending node (Claverie et al., 2018; Main-Knorn et al., 2017; Traganos & Reinartz, 2018). This local time was chosen as a compromise to minimise cloud cover and obtain appropriate solar lighting (Spoto et al., 2012). The time approximates to the local Landsat recording time and exactly matches the SPOT recording time, which allows for a combination of Sentinel-2 data and historical imagery to construct long-term time series (Claverie et al., 2018; Gascon et al., 2014; Martimort et al., 2007). Table 1 shows a comparison between Sentinel-2A and Sentinel-2B wavelengths (Doshi et al., 2020). The satellites have different wavelength centres, although the difference is not great. For comparison, the bandwidth between bands is also mostly the same, although there are some differences, namely band 5 (1 nm), band 8a (1 nm), band 9 (1 nm), band 10 (1 nm), band 11 (3 nm), band 11 (3 nm), and band 12 (10 nm).
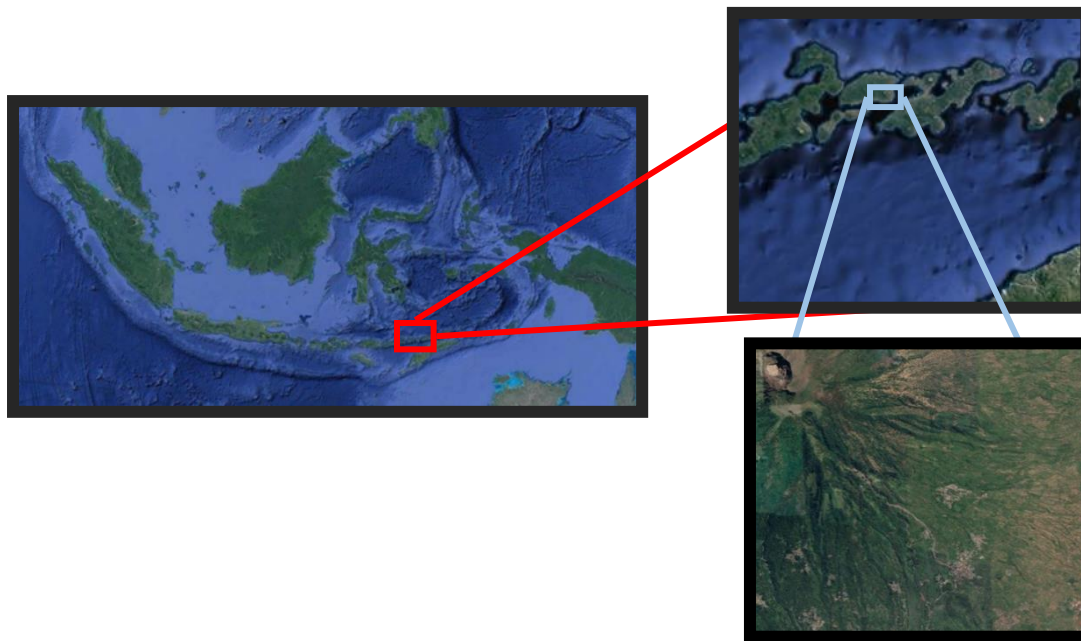
Figure 2-1. Study area, Desa Nelelamadike, Kecamatan Ile Boleng,

Table 2-1: Spectral bands for the SENTINEL-2 sensors (S2A & S2B) (Doshi et al., 2020)

| Band Number	S2A		S2B		Spatial resolution (m)
	Central wavelength (nm)	Bandwidth (nm)	Central wavelength (nm)	Bandwidth (nm)	
1	442.7	21	442.3	21	60
2	492.4	66	492.1	66	10
3	559.8	36	559.0	36	10
4	664.6	31	665.0	31	10
5	704.1	15	703.8	16	20
6	740.5	15	739.1	15	20
7	782.8	20	779.7	20	20
8	832.8	106	833.0	106	10
8a	864.7	21	864.0	22	20
9	945.1	20	943.2	21	60
10	1373.5	31	1376.9	30	60
11	1613.7	91	1610.4	94	20
12	2202.4	175	2185.7	185	20
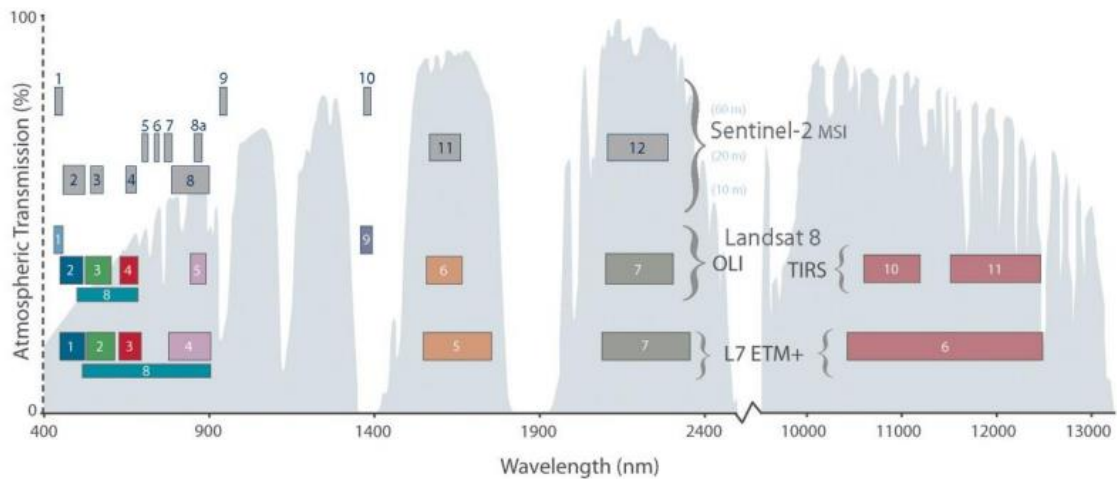
Figure 2-2. Band comparison between Sentinel-2, Landsat-8, and Landsat-7

If we compare the Sentinel-2 imagery channels with those of Landsat-8, it can be seen that several channels from Sentinel-2 are similar, namely band 1 (ocean), band 2 (blue), band 3 (green), band 4 (red), band 8a (NIR), band 11 (SWIR-1), and band 12 (SWIR-2).

Sentinel-2 data are then preprocessed so that the surface reflectance value is obtained using the sen2cor method. Sen2Cor is a Level-2A processor whose main objective is to correct single-date Sentinel-2 Level-1C Top-Of-Atmosphere (TOA) products from atmospheric influences to obtain Level-2A Bottom-Of-Atmosphere (BOA) reflectance products, with additional outputs in the form of an Aerosol Optical Thickness (AOT) map, a Water Vapor (WV) map and a Scene Classification (SCL) map with Quality Indicators for cloud and snow probabilities (Main-Knorn et al., 2017). Figure 2-3 shows the processing process from the Sentinel-2 data level-1C product into a level-2A product (Ferran Gascon et al., 2017)

In this study, band 8a was used instead of band 8 after consideration of the wavelength; as shown as Table 1, band 8 has wider bandwidth, which is wide enough to intersect with band 7 and encompass band 8a.

2.3 Sample

Determination of disaster-affected locations was made by observing such locations using high spatial resolution optical image data. Based on data from the Indonesian Topographical Map (RBI) from 2018 with a scale of 1:25000, and as shown in Figure 2-4, the affected land cover in Nelelamadike Village was mostly settlements and shrubs, with the location of the incident being a dry river. The vegetation in the incident area is sparse and dries up during the dry season. Some of the selected locations were previously residential areas and river areas, which contain shrubs during the dry season. Fifteen sample points were used for the built-up area and 15 for the scrub area. Some examples of the location of sample points before and after the flash flood incident can be seen in Figure 2-5.

From each of these points, temporal image selection was then made, as sometimes the sample location will be covered by cloud that interferes with the monitoring. The temporal image specification used was the image closest to the date of the incident (4 April 2021), both

in the images before and after the flash flood disasters. The selected image was a cloud-free image, which in Sentinel-2 can be determined with the help of the QA60 band (Corbane et al., 2020). QA60 is a band on Sentinel-2 with a resolution of 60 m (Traganos & Reinartz, 2018) and is generated by the blue band and two short-wave infrared bands of Sentinel-2 images.

However, the effect of cloud detection is unstable, which usually leads to underestimation or overestimation (Li et al., 2021). The cloud-free value in the QA60 band is marked with a value of 0 on the pixel, while a value of 1 indicates a dense cloud pixel, and a value of 2 indicates a cirrus cloud pixel (Coluzzi et al., 2018).
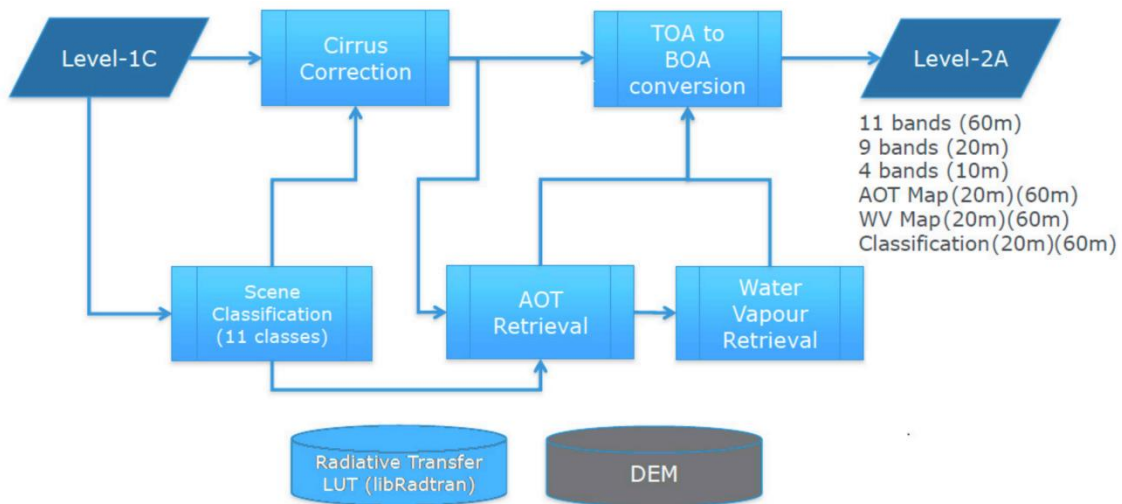
Figure 2-3. Preprocessing data from Sentinel-2 Level-1C to Sentinel-2 Level
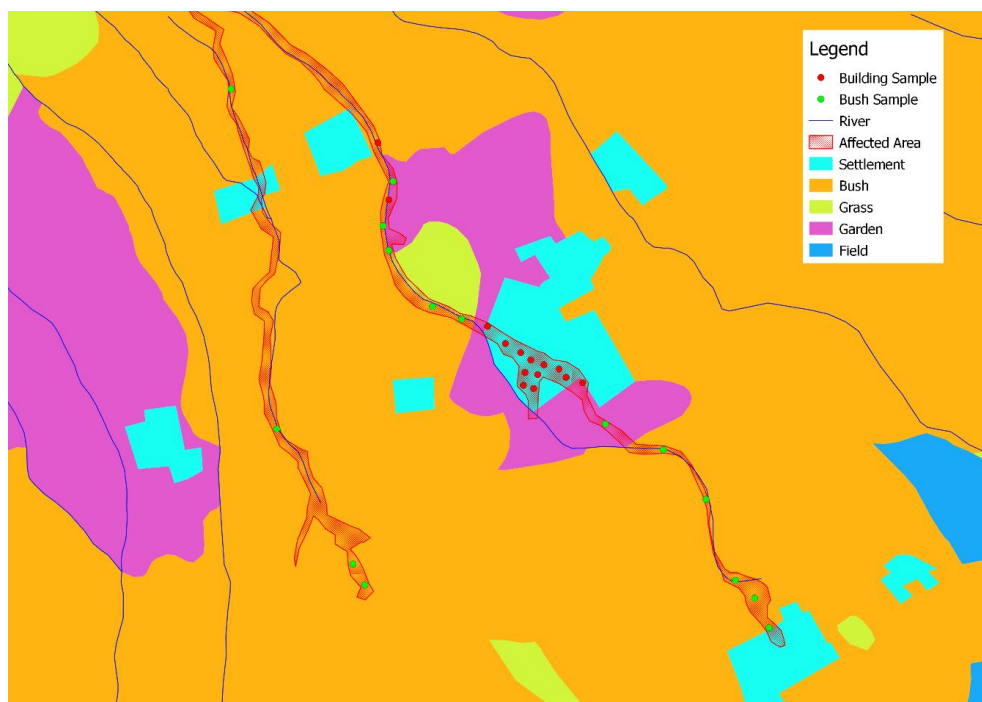

Figure 2-4. LULC (2018) affected areas in Nelelamadike village and sample

Figure 2-5. Locations affected by flash floods: before (left) and after (right).

2.4 Analysis Methods

Figure 2-6 shows a flowchart of the method used to obtain the reflectance value of flash flood events. From all the cloud-free sample points, the average calculation for each channel was then made for the same observation time. The average calculation can use the equation 1.

$$\tilde{x} = \frac{1}{n}\left(\sum_{i=1}^{n} x_i\right) \qquad (2\text{-}1$$

where $\tilde{x}$ is the average; n is the number of data; and x_i is reflectance at data i. Subsequently, observations were made between the reflectance before and after the incident, and then the data analysis was performed.
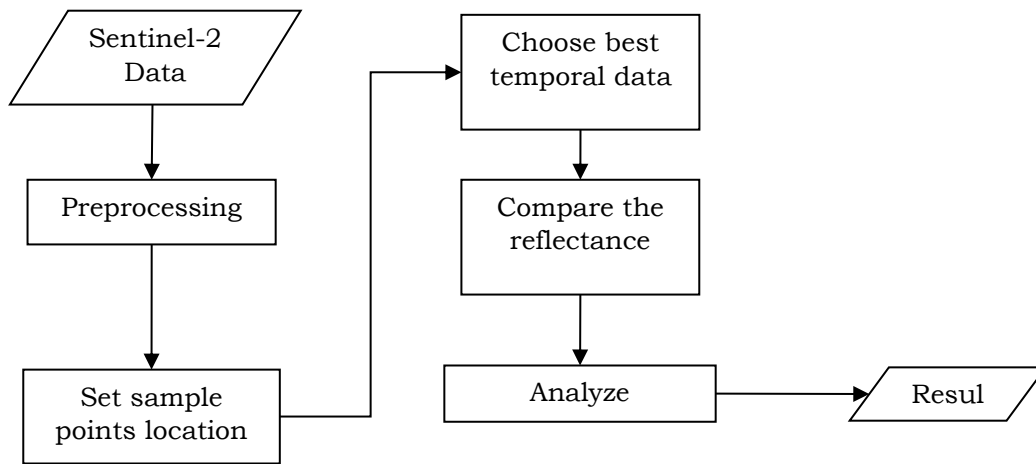
Figure 2-6. Flowchart of the research method used in determining the reflectance value.

3   RESULTS AND DISCUSSION

3.1 Differences in reflectance in settlement areas before and after flash flood incidents

Figure 3-1 shows the reflectance comparison before and after flash flood incidents in the settlement area. It can be seen that the reflectance value of post-disaster events is lower than that of pre-disaster events in all bands. In this flash flood incident, the object before the disaster was a building, but afterwards it was vacant land. Compared with the reflectance graph in Figure 3-2 (Surase et al., 2019), the reflectance results shown in Figure 3-1 are fairly different. In this figure the reflectance of buildings (urban) is higher than that of soil, but in Figure 3-2, it can be seen that the reflectance of urban areas is much lower than that of soil. The reflectance of the soil in Figure 3-2 can reach around 60% for visible, NIR, and SWIR bands, but that caused by flash floods only has a maximum of around 20% at NIR, with a range of around from 5% to 20%.

The low soil reflectance obtained, as shown in Figure 3-1, is most likely due to the influence of existing soil moisture, which may consist 4 days after the flash flood event. In research on the reflectance on beach sand with various humidity levels, it has been shown that the more humid the conditions, the lower the reflectance level, as shown in Figure 3-3 (Nolet et al., 2014). This can be analogous to the soil condition; if the soil is wet, the reflectance value will be lower, causing the reflectance value of the soil itself to be lower than the reflectance value of urban areas.

Figure 3-4 shows the reflectance values before and after the flood incident in the residential area. The reflectance pattern of the bush area and objects in the residential area show the same significant changes in band 6 to band 8A. This gives satisfactory results to explain that the change in the reflectance value in the object of the residential area is significant. Bands 6 to 8A are red-edge and NIR narrow band.

Comparison of Reflectance Before and After the Flash Flood
in the Impacted Settlement Area (Mean)
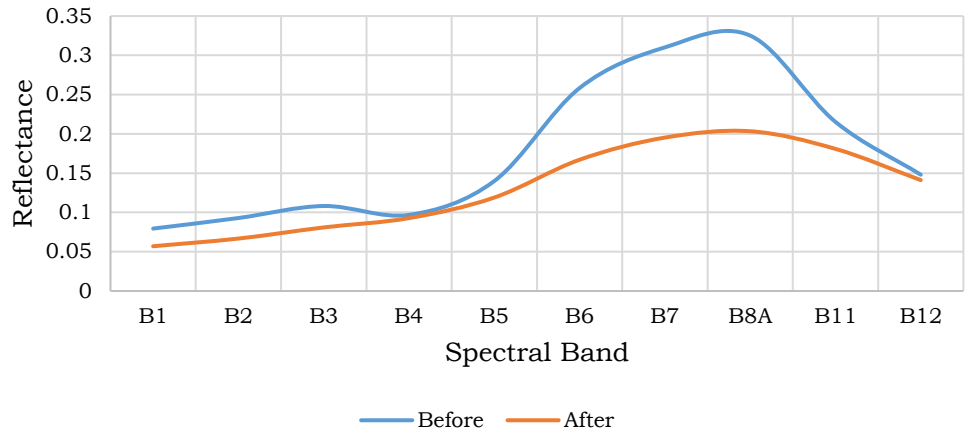
Comparison of Reflectance Before and After the Flash Flood
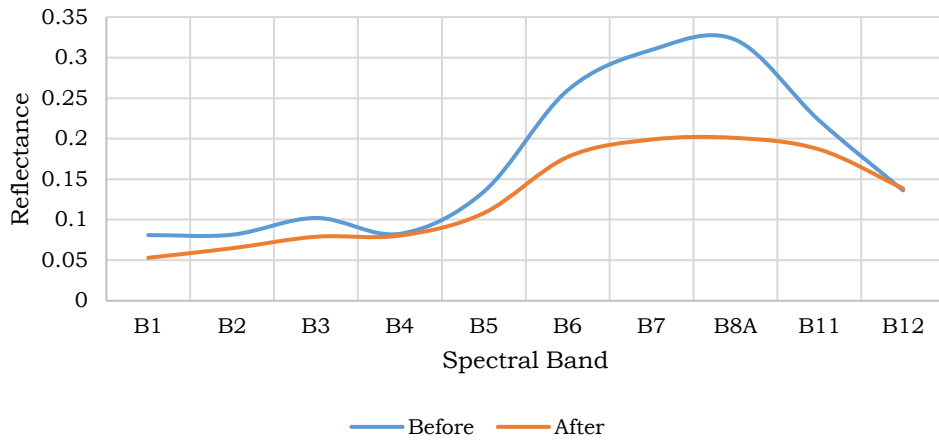in the Impacted Settlement Area (Median)

Figure 3-1: Reflectance comparison in the settlement area before and after the incident: mean (above) and median (below).
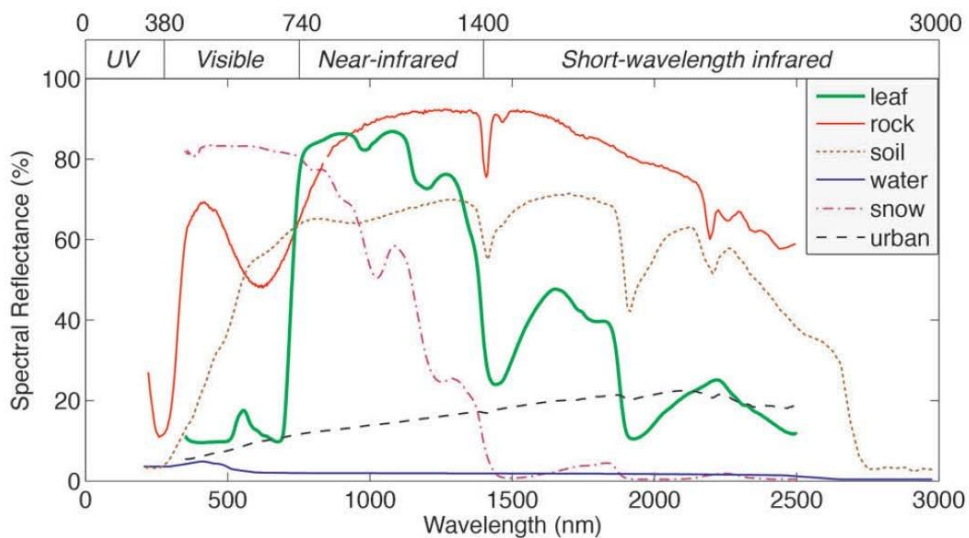

Figure 3-2. Reflectance of different objects on the earth's surface (Surase et al., 2019)
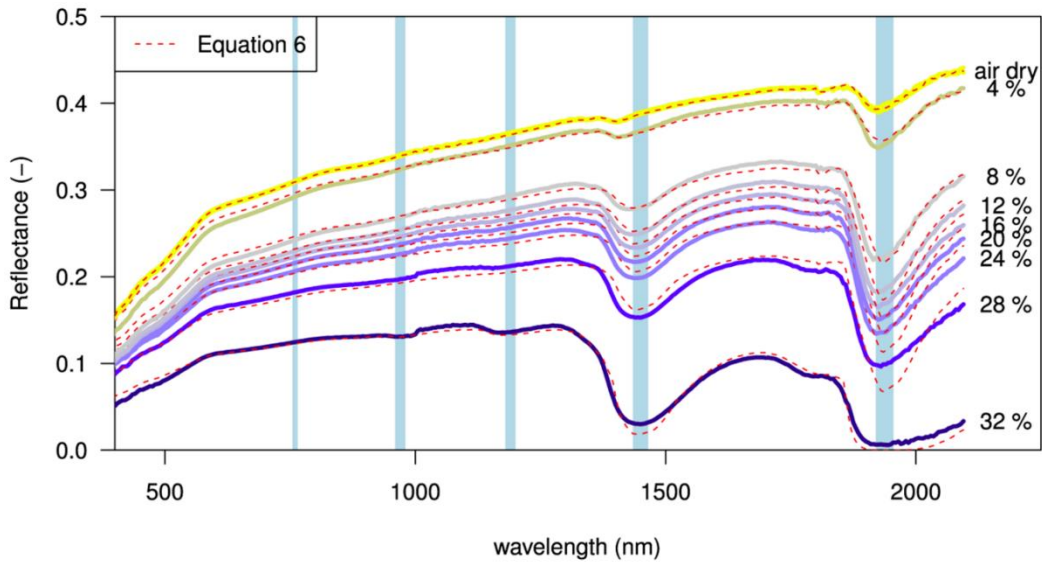
Figure 3-3. Beach sand reflectance with different levels of moisture (Nolet et al., 2014)
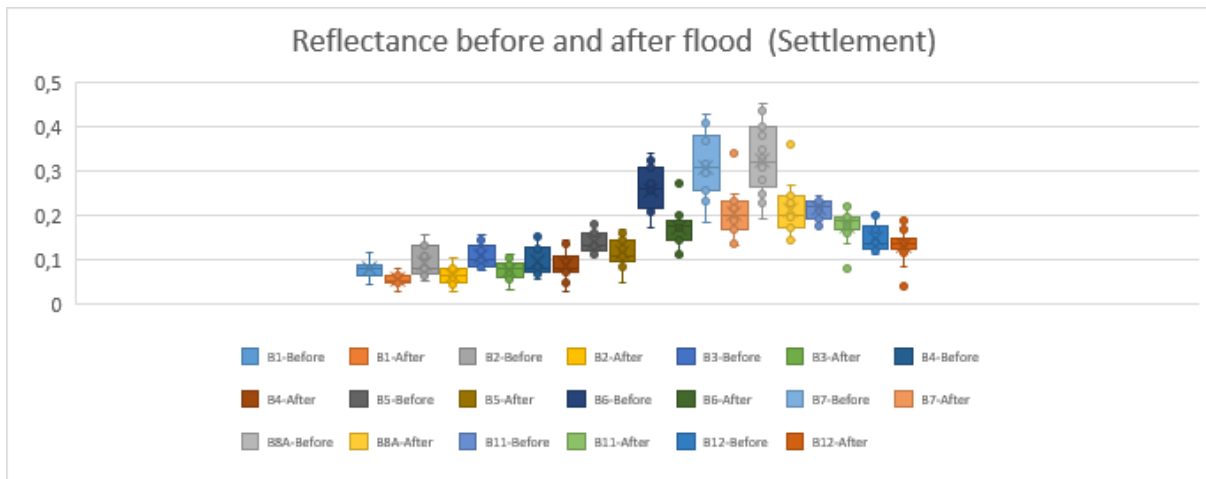

Figure 3-4   Reflectance differences in the settlement before and after the flash flood incident, showing a significance difference in bands 6 to 8a.

3.2 Reflectance differences in the bush area before and after the incident

Figure 3-5 shows a comparison between the reflectance before and after the flash flood in the bush area, which is actually in a waterway or river that is dry during the dry season. As shown in Figure 3-5, it can be seen that the reflectance of the bush is similar to that of the residential area, but that the reflectance value is higher. The condition of the affected area after the event also appears higher for the infrared bands than the affected residential areas. Seeing that the conditions in the study area are dry, the vegetation may be dry. A comparison between the reflectance from the dry vegetation and the soil can be seen in Figure 3-5 (Verhoeven & Loenders, 2006).

From Figure 3-6, it can be seen that the reflectance pattern of dry vegetation is more similar to the reflectance of the soil than that of the green vegetation. The reflectance pattern of dry vegetation is more similar to the reflectance of the soil

than that of the green vegetation. The reflectance of the dry vegetation looks higher than the reflectance of the ground, which is also seen in Figure 3-4, where the condition before the incident, which is characterised by bush or dry vegetation, has a reflectance pattern that is similar to that after the incident (soil) with different reflectance levels.

By performing calculations and statistical analysis of the bush and settlement objects before and after the flood incident, it can be seen that the wavelengths that show a very significant difference are bands 6 to 8A. Figure 3-7 shows the reflectance values before and after the flood event in the bush area. The pattern in bands 6 to 8A gives satisfactory results to explain that the change in the reflectance value in the bush region object changes significantly.
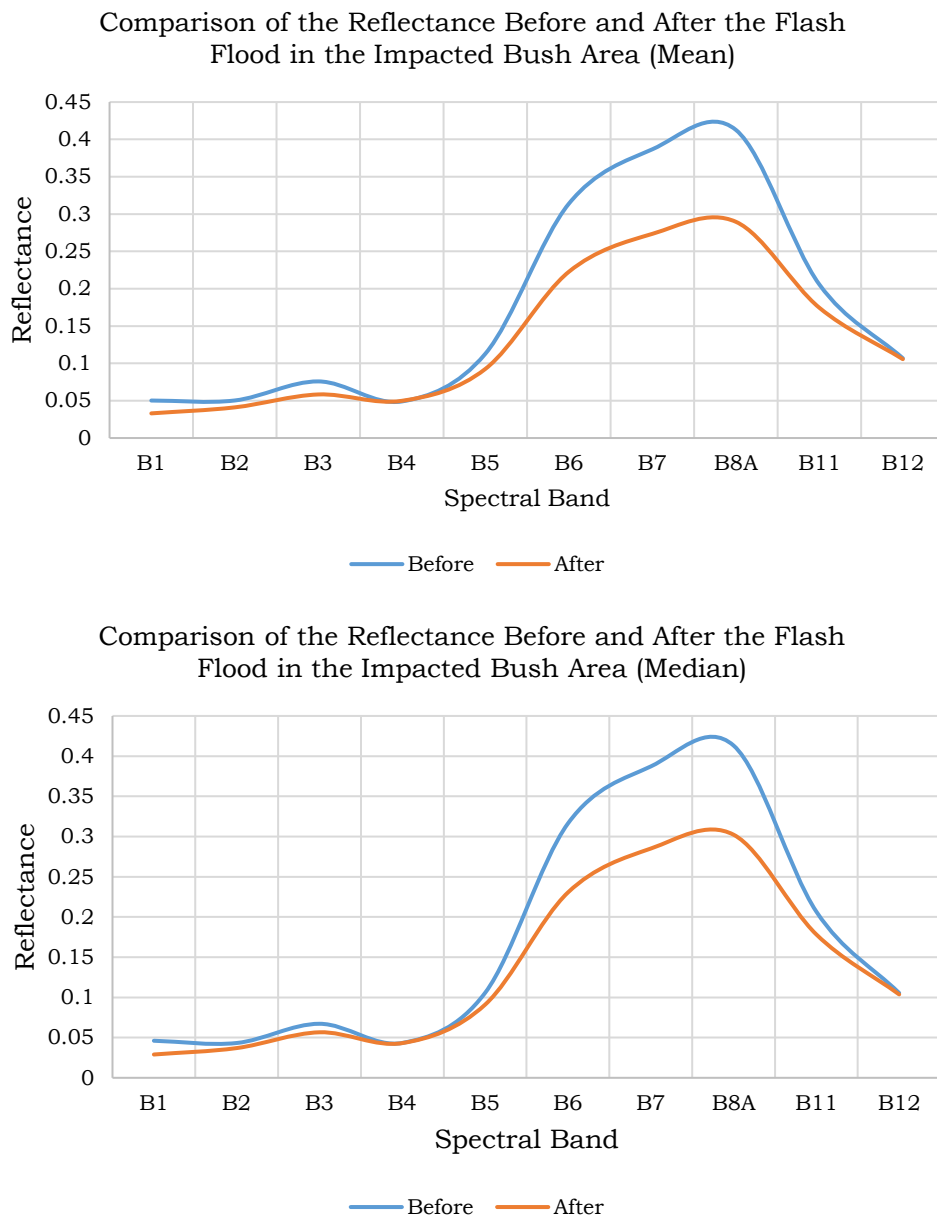

Comparison of the Reflectance Before and After the Flash Flood in the Impacted Bush Area (Mean)

Comparison of the Reflectance Before and After the Flash Flood in the Impacted Bush Area (Median)

Figure 3-5   Reflectance comparison of the bush area before and after the flash flood incident: mean (above) and median (below).
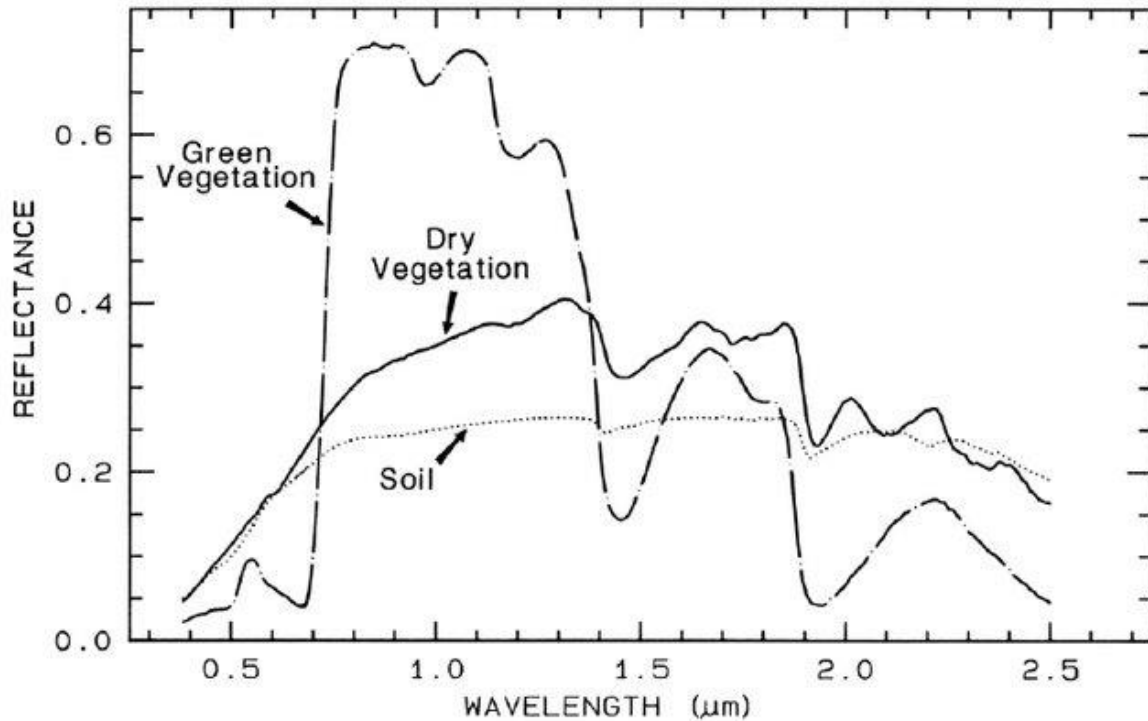
.

Figure 3-6   Soil, green vegetation, and dry vegetation reflectance comparison (Verhoeven & Loenders, 2006).
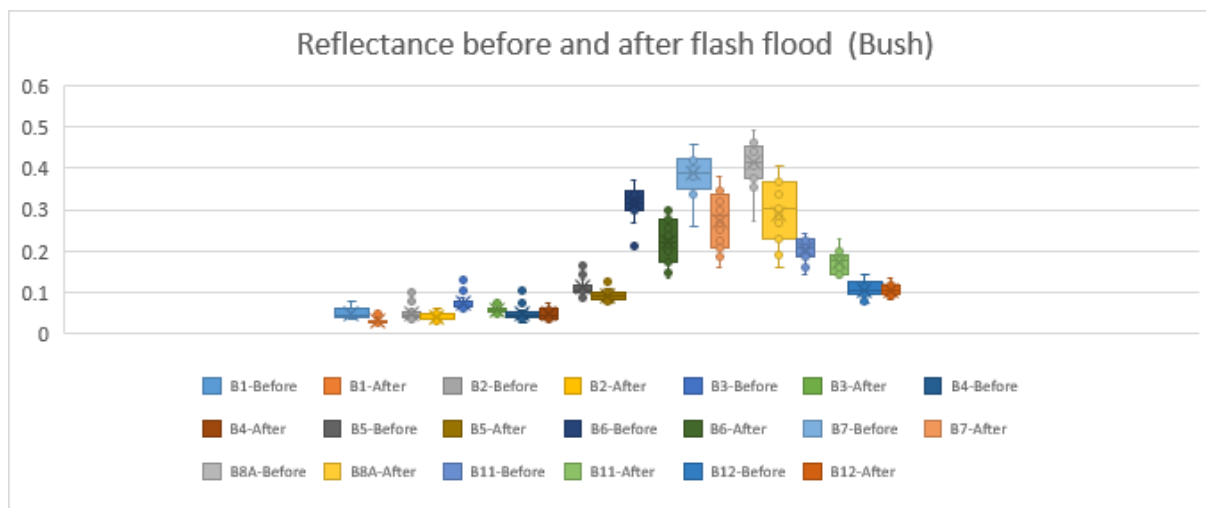

Figure 3-7   Reflectance difference in the bush area before and after the flash flood incident, showing a significance difference in bands 6 to 8A..

4   CONCLUSIONS

From the observations of the reflectance of the flash flood disaster in Nelelamadike Village, East Flores Regency, East Nusa Tenggara caused by the Seroja tropical storm, it can be seen that the condition of the affected area has a reflectance pattern of soil with high humidity. The area, which was previously bush and a residential area, appears to have a reflectance pattern that is similar to that after the incident, which was open ground on the basis of the Sentinel-2 satellite imagery data. It is concluded that

Sentinel-2 channels 6, 7, and 8A have significant differences compared to the other channels regarding differences in reflectance before and after the flooding in relation to both the settlement and bush areas. These results could be used for further research in building a reflectance index for the rapid detection of affected areas which focuses on these channels.

ACKNOWLEDGEMENTS

AUTHOR CONTRIBUTIONS

Project leader: MP; conceptualization and methodology: SKW, MRK, and MP; writing and preparation of original draft: MP and GAC; data processing: GAC and MP; formal analysis: MRK and MP; validation: GAC and MP; writing, review and editing: SKW, MRK, and MP.

REFERENCES

Ali, A., Adrianto, R., & Saepudin, M. (2019). Preliminary Study Of Horizontal And Vertical Wind Profile Of Quasi-Linear Convective Utilizing Weather Radar Over Western Java Region, Indonesia. International *Journal of Remote Sensing and Earth Sciences (IJReSES), 15*(2), 177-186.

Ali, A., Deranadyan, G., & Umam, I. H. (2020). An Enhancement to The Quantitative Precipitation Estimation Using Radar-Gauge Merging. *International Journal of Remote Sensing and Earth Sciences (IJReSES), 17*(1), 65-74.

Ali, A., Supriatna, S., & Sa'adah, U. (2021). Radar-Based Stochastic Precipitation Nowcasting Using The Short-Term Ensemble Prediction System (Steps)(Case Study: Pangkalan Bun Weather Radar).

International Journal of Remote Sensing and Earth Sciences (IJReSES), 18(1), 91-102.

Breiman, L. (2001). Random forests. *Machine Learning, 45*(1), 5-32.

Cho, J. Y. (2017). A new radio frequency interference filter for weather radars. Journal of Atmospheric and Oceanic *Technology*, 34(7), 1393-1406.

Doviak, R. J., Zrnic, D. S., & Sirmans, D. S. (1979). Doppler weather radar. *Proceedings of the IEEE, 67*(11), 1522-1553.

Firdaus, T., & Suryadi, D. (2019). Analisis Interferensi Frekuensi Radio Radar Cuaca Badan Meteorologi Klimatologi Dan Geofisika (BMKG) Di Kalimantan Barat. *Jurnal Teknik Elektro Universitas Tanjungpura, 2*(1).

Ginting, S. (2014). Sistem peringatan dini banjir Jakarta. *Jurnal Sumber Daya Air, 10*(1), 71-84.

Hailong, W., Shouyuan, D., Xu, W., & Zhao, S. (2019, December). Sea clutter recognition based on dual-polarization weather radar. *In 2019 International Conference on Meteorology Observations (ICMO)* (pp. 1-3). IEEE.

Hubbert, J. C., Dixon, M., Ellis, S. M., & Meymaris, G. (2009). Weather radar ground clutter. Part I: Identification, modeling, and simulation. *Journal of Atmospheric and Oceanic Technology, 26*(7), 1165-1180.

ITU-R Radio Communication Study Groups, documents 8A/103-E and 8B/65-E, August 30, 2004. *Studies on the effect of wireless access systems including RLANs on terrestrial meteorological radars operating in the band 5600-5650 MHz.* International Telecommunication Union (ITU), Geneva, Switzerland.

Joe, P., Scott, J., Sydor, J., Brandão, A., & Yongacoglu, A. (2005, October). Radio local area network (RLAN) and C-band weather radar interference studies. *In Proc. 32nd*

AMS Radar Conference on Radar Meteorology.

Keränen, R. E. I. N. O., Rojas, L., & Nyberg, P. E. T. R. I. (2013). Progress in mitigation of WLAN interferences at weather radar. *In 36th Conf. on Radar Meteorology.*

McRoberts, D. B., & Nielsen-Gammon, J. W. (2017). Detecting beam blockage in radar-based precipitation estimates. *Journal of Atmospheric and Oceanic Technology, 34*(7), 1407-1422.

Moon, J., & Ryu, C. (2017). WiFi (RLAN) and a C-Band Weather Radar Interference. *Journal of the Chosun Natural Science, 10*(4), 216-224.

Pal, M. (2005). Random forest classifier for remote sensing classification. *International Journal of Remote Sensing, 26*(1), 217-222.

Rojas, L., Moisseev, D. N., Chandrasekar, V., Selzler, J., & Keränen, R. (2012). Dual-polarization spectral filter for radio frequency interference suppression. *In Preprints, Seventh European Conf. on Radar in Meteorology and Hydrology (ERAD 2012), Toulouse, France.* Météo-France.

Saltikoff, E., Cho, J. Y., Tristant, P., Huuskonen, A., Allmon, L., Cook, R., Becker, E., & Joe,P. (2016). The threat to weather radars by wireless technology. *Bulletin of the American Meteorological Society, 97*(7), 1159-1167.

Wardoyo, E. (2014). Analisis Interferensi Frekuensi Radar Cuaca C-Band di Indonesia. *InComTech: Jurnal Telekomunikasi dan Komputer, 5*(2), 163-184.

Yin, J., Chen, H., Li, Y., & Wang, X. (2021). Clutter Mitigation based on Spectral DepolarizationRatio for Dual-polarization Weather Radars. *IEEE Journal of Selected Topics in Applied Earth Observations and Remote Sensing.*